Paper I

AAC Journals.ASM.org

His224 Alters the R2 Drug Binding Site and Phe218 Influences the Catalytic Efficiency of the Metallo-β-Lactamase VIM-7

Hanna-Kirsti S. Leiros,[a] Susann Skagseth,[a] Kine Susann Waade Edvardsen,[a]* Marit Sjo Lorentzen,[a]* Gro Elin Kjæreng Bjerga,[a]* Ingar Leiros,[a] Ørjan Samuelsen[b]

The Norwegian Structural Biology Centre (NorStruct), Department of Chemistry, UiT The Arctic University of Norway, Tromsø, Norway[a]; Reference Centre for Detection of Antimicrobial Resistance, Department of Microbiology and Infection Control, University Hospital of North Norway, Tromsø, Norway[b]

Metallo-β-lactamases (MBLs) are the causative mechanism for resistance to β-lactams, including carbapenems, in many Gram-negative pathogenic bacteria. One important family of MBLs is the Verona integron-encoded MBLs (VIM). In this study, the importance of residues Asp120, Phe218, and His224 in the most divergent VIM variant, VIM-7, was investigated to better understand the roles of these residues in VIM enzymes through mutations, enzyme kinetics, crystal structures, thermostability, and docking experiments. The tVIM-7-D120A mutant with a tobacco etch virus (TEV) cleavage site was enzymatically inactive, and its structure showed the presence of only the Zn1 ion. The mutant was less thermostable, with a melting temperature (T_m) of 48.5°C, compared to 55.3°C for the wild-type tVIM-7. In the F218Y mutant, a hydrogen bonding cluster was established involving residues Asn70, Asp84, and Arg121. The tVIM-7-F218Y mutant had enhanced activity compared to wild-type tVIM-7, and a slightly higher T_m (57.1°C) was observed, most likely due to the hydrogen bonding cluster. Furthermore, the introduction of two additional hydrogen bonds adjacent to the active site in the tVIM-7-H224Y mutant gave a higher thermostability (T_m, 62.9°C) and increased enzymatic activity compared to those of the wild-type tVIM-7. Docking of ceftazidime in to the active site of tVIM-7, tVIM-7-H224Y, and VIM-7-F218Y revealed that the side-chain conformations of residue 224 and Arg228 in the L3 loop and Tyr67 in the L1 loop all influence possible substrate binding conformations. In conclusion, the residue composition of the L3 loop, as shown with the single H224Y mutation, is important for activity particularly toward the positively charged cephalosporins like cefepime and ceftazidime.

The carbapenems belong to the β-lactam class of antibiotics and are one of the last-line drugs for treatment of patients infected with multidrug-resistant Gram-negative bacilli (1–4). The most widespread mechanism for carbapenem resistance is the presence of carbapenemases, β-lactamases that are able to hydrolyze carbapenems (3, 5, 6). Carbapenemases can be found among both serine β-lactamases (molecular classes A and D) and metallo-β-lactamases (MBLs) (molecular class B) (7). The MBLs are a diverse family of β-lactamases that includes mobile MBLs, such as VIMs, NDMs, IMPs, and SPM, which are either globally distributed or highly prevalent in certain regions (1, 6, 8–10). MBLs can be divided into four subclasses (B1a, B1b, B2, and B3) according to their structure and molecular characteristics (11, 12). The MBLs are efficient carbapenemases but also have activity against penicillins and cephalosporins but not monobactams (5). MBLs are now found in many different Gram-negative bacterial species, and the presence of an acquired MBL is often associated with resistance to other classes of antibiotics, resulting in multidrug resistance, limiting the treatment options for infected patients (1–3).

The VIM family is a large family of MBLs that currently includes 41 different VIM-variants (http://www.lahey.org/Studies/) which can be divided into three subgroups: VIM-1, VIM-2, and VIM-7 (13). VIM-7, identified in *Pseudomonas aeruginosa*, was first reported in a clinical isolate from the United States of America in 2001 (14) and is the most divergent VIM enzyme, with only 74% and 77% sequence identity to VIM-1 and VIM-2, respectively. We previously determined the enzyme kinetics (15) and the three-dimensional structure of VIM-7 (16). The enzyme kinetics showed VIM-7 to be an efficient penicillinase and carbapenemase, but VIM-7 displayed variable cephalosporinase activity compared to VIM-1 and VIM-2, with lower activity against cephalosporins having bulky and positively charged C-3 substituents (15).

The detailed reaction mechanism of MBLs seems to be substrate dependent, and the exact role of the metal ion(s) remains controversial (17, 18). Still, Asp120 is conserved in both the dizinc B1 and B3 subclasses, which contain zinc in both the Zn1 (trihistidine) and Zn2 (Asp-Cys/His-His) sites, and in the monozinc B2 subclass, which mainly contains zinc in the Zn2 site (17). Asp120 binds to both Zn2 and the bridging hydroxyl ion in, e.g., the VIM-2, VIM-4, and VIM-7 structures (16, 19, 20). During catalysis, Asp120 probably orients the new hydroxyl ion after catalysis and keeps the correct orientations in the protonation step during cleavage of the C-N bond in the four-member β-lactam ring (17, 21). The resulting negatively charged tetrahedral intermediate is then stabilized by interactions with the metal, and Asp120 donates a proton to the nitrogen atom in the substrate, resulting in open-

Received 16 December 2013 **Returned for modification** 28 January 2014
Accepted 1 June 2014
Published ahead of print 9 June 2014

Address correspondence to Hanna-Kirsti S. Leiros, hanna-kirsti.leiros@uit.no.

* Present address: Kine Susann Waade Edvardsen, Department of Clinical Science, Section for Endocrinology, University of Bergen, Bergen, Norway; Marit Sjo Lorentzen, ArcticZymes AS, Tromsø, Norway; Gro Elin Kjæreng Bjerga, Uni Research AS, Centre for Applied Biotechnology, High Technology Centre, Bergen, Norway.

Supplemental material for this article may be found at http://dx.doi.org/10.1128/AAC.02735-13.

doi:10.1128/AAC.02735-13

TABLE 1 List of primers used for tVIM-7 cloning, site-directed mutagenesis, and sequencing

Primer name	Sequence (5′→3′)[a]	T_m (°C)[b]
VIM-7-fwd	*CAT CAC CAT CAC CAT CAC* **GAA AAC CTG TAT TTC CAG GGA GCA** GCA CAG CCT GGC GGT GAA TAT CCG	76.5
VIM-7-rev *att*B2	GGG GAC CAC TTT GTA CAA GAA AGC TGG GTC TTA CTC GGC CAC CGG GCG TAC TTT G	75.8
*att*B1-His-fwd	G GGG ACA AGT TTG TAC AAA AAA GCA GGC TTC GAA GGA GAT AGA ACC ATG *CAT CAC CAT CAC CAT CAC*	73.8
F218Y-Forward	C GTG CGC GTA CTG **TAT** GGT GGC TGT GCA G	67.2
F218Y-Reverse	C TGC ACA GCC ACC **ATA** CAG TAC GCG CAC G	67.2
H224Y-Forward	TGT GCA GTT **TAT** GAG GCG TCA CGC GAA TCC GCG GGT AAT GTT GCC	72.7
H224Y-Reverse	TGA CGC CTC **ATA** AAC TGC ACA GCC ACC AAA CAG TAC GCG CAC GG	72.9
D120A-Forward	CAC TTC CAT GAC **GCT** CGA GTC GGT GGA	64.3
D120A-Reverse	TCC ACC GAC TCG **AGC** GTC ATG GAA GTG	64.3
M13 forward	GTA AAA CGA CGG CCA GT	47.1
M13 reverse	GGA AAC AGC TAT GAC CAT G	48.9
T7 promoter	TAA TAC GAC TCA CTA TAG GG	47.7
T7 terminator	GCT AGT TAT TGC TCA GCG G	51.1

[a] The positions of mutations are given in boldface and underlined for each primer, the His tag is given in italic, the TEV protoease site is given in boldface, and the *att*B sites are underlined.
[b] The melting temperature was calculated using the website http://insilico.ehu.es/tm.php.

ing of the β-lactam ring (17). Several mutants of Asp120 in the class B3 MBL enzyme L1 from *Stenotrophomonas maltophilia* showed a 10- to 1,000-fold decrease in k_{cat} compared to wild-type L1, and thus, Asp120 was confirmed to play a significant role in the hydrolysis reaction (22, 23). This has also been shown for IMP-1 (24), CphA (25), and BcII (26). To study the role and importance of Asp120 in VIM-7 for zinc binding, thermostability, and catalysis, a D120A mutant was created and analyzed.

Two anti-parallel β-strands connected by a loop determine the L1 loop (residues 60 to 66) and are proposed to form a lid over the active site in several class B1 MBLs, including GIM-1 (27), VIM-7 (16), and IMP-1 (28–30). For the latter, the mutation of F218Y increased the catalytic efficiency compared to that of wild-type IMP-1 through hydrogen bond formation, improving the closing-down movement of this lid (28, 29). We therefore decided to make the same mutation in VIM-7 (F218Y) to analyze the effect of additional hydrogen bonds on the structure and enzyme activity despite the low amino acid sequence identity between VIM-7 and IMP-1 of 28%. The mutation was also selected since the structure analysis of VIM-7 suggested that residue 218 was one possible residue determinant implicated in the reduced catalytic efficiency of VIM-7 compared to VIM-2, particularly for cephalosporins with a positively charged cyclic substituent at the C-3 position, like ceftazidime and cefepime (15, 16). The hydrogen binding cluster in VIM-2 from Tyr218 OH to Asn70 O, to the invariant Asp84 OD2, and to Arg121 NH1, is absent in VIM-7 due to Phe218 and results in a proposed increased flexibility and reduced activity of VIM-7 (16).

Structural analysis pointed to His224 as being partly responsible for the reduced activity of VIM-7. Residue 224 is part of a loop that includes residues 223 to 240, called L3, L10, or loop 2 (herein denoted L3) (31). In VIM-2, tyrosine is present at position 224, and in the folded protein, this residue protrudes into the R2 binding site of the antibiotic (19, 20). Furthermore, the Tyr224 OH atom in VIM-2 forms two hydrogen bonds—one that interacts via a water molecule with the Zn1 ligand His196 and one that interacts with Gly232 N (16, 19, 20). These hydrogen bonds and interactions are absent in VIM-7 and VIM-4 due to the presence of histidine at this position (16, 20). Residue 224 is a conserved lysine in many B1 family MBLs and was found to be critical for binding the carboxyl group on the C-3/C-4 atom of the substrate (21, 32, 33). Here we created a H224Y mutant to investigate the role of residue 224 in the structure, enzymatic activity, and thermostability of VIM-7 and the importance of potential additional hydrogen bonds.

To summarize, we have investigated the VIM-7 structure further by structure-activity relationship (SAR) through mutational analysis of three residues: Asp120, Phe218, and His224. The mutants were investigated with respect to enzyme kinetics, crystal structures, thermostability assays, and docking experiments. Asp120 was found to be crucial for the enzyme activity and stability, and the crystal structure showed tVIM-7-D120A to be a monozinc enzyme. Both F218Y and H224Y mutants had additional hydrogen bonds compared to the wild-type tVIM-7 structure, as expected: the melting temperature was increased by 1.8°C (F218Y) and 7.6°C (H224Y), and an increased k_{cat} was found for many substrates. This indicates that residue 224 in the L3 loop and residue 218 are both important residue determinants for activity and stability for the VIM family of enzymes.

MATERIALS AND METHODS

Cloning of tVIM-7. In this study, two different recombinant VIM-7 constructs were used. One construct contained the native VIM-7 gene, bla_{VIM-7}, from *Pseudomonas aeruginosa* (GenBank accession no. Q840P9) expressed in pET26b(+) (Novagen) with the native leader sequence and purified from the periplasm as described earlier (16). This recombinant protein will be referred to as VIM-7. To obtain a higher yield of recombinant protein, we generated another construct encoding *P. aeruginosa* VIM-7 (residues Ala25 to Glu300) in pDEST14 (Invitrogen), where the predicted leader sequence and eight extra residues were replaced with an N-terminal, tobacco etch virus (TEV) protease-cleavable His tag. This recombinant protein is referred to as tVIM-7. The class B β-lactamase (BBL) numbering system is used throughout this paper for numbering of all residues (34).

The gene sequence coding for residues Ala25 to Glu300 in VIM-7 was amplified with the VIM-7-fwd and VIM-7-rev *attB2* primers (Table 1), using the VIM-7/pET26b(+) construct as the template. A Phusion PCR was done consisting of 1× HF buffer, 200 μM deoxynucleoside triphosphate (dNTP) mix, 0.5 μM forward primer, 0.5 μM reverse primer, approximately 100 ng VIM-7/pET26b(+) template, 1 μl (0.02 U) Phusion polymerase, and nuclease-free water. Amplification was performed with the following cycle conditions: initial denaturation at 95°C for 5 min, followed by 30 cycles of denaturation at 95°C for 30 s, annealing at 55°C for 30 s, and elongation at 72°C for 45 s, followed by a final extension at

72°C for 5 min. The PCR product was confirmed by agarose gel electrophoresis.

One microliter of the PCR product was then used as a template in a second amplification using the *att*B1-His-fwd and the VIM-7-rev *att*B2 primers (Table 1). A new Phusion PCR was done with the same cycle conditions as described above. The resulting PCR product was used in the BP recombination reaction (recombination between *att*B and *att*P sites) to generate an entry clone in the pDONR221 vector (Invitrogen) followed by transformation of *Escherichia coli* DH5α (Invitrogen) with the construct. Sequencing, using the BigDye Terminator v3.1 technology (Applied Biosystems) and M13 primers flanking the insert (Table 1), was performed to confirm the cloning. The entry clone was subsequently transferred to the pDEST14 vector in an LR recombination reaction (recombination between *att*L and *att*R sites) to generate the expression clone.

Construction of VIM-7 mutants by site-directed mutagenesis. The QuikChange site-directed mutagenesis kit (Agilent Biosciences) was used to generate the D120A, H224Y, and F218Y mutants of VIM-7 according to the manufacturer's protocol. Primers were designed to introduce the desired mutations (Table 1). Parental DNA was digested with DpnI, and *E. coli* XL1-Blue cells (Agilent Biosciences) were transformed with the PCR products for clone selection. Mutations were verified by DNA sequencing as described above, using insert flanking T7 primers (Table 1). The H224Y, D120A, and F218Y mutants were made using the tVIM-7/pDEST14 template (tVIM-7 mutants) and a second F218Y mutant used the VIM-7/pET26b(+) template.

Expression and purification. The VIM-7 and VIM-7-F218Y constructs were transformed into *E. coli* BL21(DE3) (Invitrogen) and grown in Terrific broth (TB) supplied with 50 mg/liter kanamycin (Sigma-Aldrich) at 37°C. Cultures were induced during the mid-log phase for 3 to 4 h at 37°C with 0.4 mM isopropyl-β-D-thiogalactopyranoside (IPTG) (Sigma). Recombinant protein was purified from the periplasm followed by ion-exchange chromatography on a Q-Sepharose HP column (GE Healthcare) and gel filtration on a Superdex 200 column (GE Healthcare) as reported earlier (16). After gel filtration, the recombinant VIM-7-F218Y mutant was diluted to obtain 1 M ammonium sulfate and applied to a HiTrap Phenyl FF hydrophobic column (GE Healthcare). Unbound protein was washed off in buffer A (1.5 M ammonium sulfate, 50 mM Tris [pH 7.2], 100 μM $ZnCl_2$), and recombinant VIM-7-F218Y was eluted with a 0 to 100% gradient of buffer B (50 mM Tris [pH 7.2], 100 μM $ZnCl_2$) and dialyzed against buffer C (50 mM HEPES [pH 7.2], 150 mM NaCl, and 100 μM $ZnCl_2$).

The TEV constructs tVIM-7 and tVIM-7-D120A were transformed into *E. coli* strain BL21 Star(DE3) (Invitrogen) and grown at 37°C in TB supplied with 50 mg/liter ampicillin (Sigma). tVIM-7-H224Y and tVIM-7-F218Y were transformed into *E. coli* Rosetta 2(DE3)/pLysS (Novagen) for expression and purification in Luria-Bertani (LB) medium with 100 mg/liter ampicillin and 34 mg/liter chloramphenicol. All TEV constructs were induced during mid-log phase with 0.4 mM IPTG, and the cells were harvested after 3 to 4 h at 37°C or after induction at 20°C overnight.

The soluble lysates of tVIM-7, tVIM-7-D120A, tVIM-7-H224Y, and tVIM-7-F218Y were, after sonication, each applied to either 1- or 5-ml HisTrap HP columns (GE Healthcare) equilibrated in buffer D (50 mM HEPES or Tris [pH 7.2] and 100 μM $ZnCl_2$). Bound proteins were washed with 5% buffer E (50 mM HEPES or Tris [pH 7.2], 100 μM $ZnCl_2$, 500 mM imidazole) and eluted across a gradient of 5 to 100% buffer E. TEV protease was expressed from a TEV pM2 plasmid (35), in which the two mutations L56V and S135G (35, 36) had been added to the four existing mutations S219N, T17S, N68D, and I77V in the pTH24:TEV_{SH} plasmid, kindly provided by H. Berglund at the Karolinska Institutet, Sweden (37). This new in-house-made TEV protease, expressed in frame with a C-terminal His tag was added to pooled fractions containing the recombinant tVIM-7 proteins in a 1:10 ratio of TEV protease to target protein in 10-kDa-cutoff SnakeSkin dialyse tubing (Thermo Scientific) and dialyzed overnight at 4°C while stirring against 10 mM HEPES or Tris (pH 7.2), 100 mM NaCl, 1 mM 2-mercaptoethanol, and 1 mM EDTA. A second HisTrap purification was performed as described above to remove contaminants, uncleaved tVIM-7 proteins, and the His-tagged TEV protease. tVIM-7-H224Y was furthermore analyzed on a Superdex HiLoad 16/60 column (GE Healthcare) in buffer F (50 mM Tris [pH 7.5], 150 mM NaCl, 100 μM $ZnCl_2$) and found to be monomeric compared to standard molecular weight proteins. After TEV protease cleavage, tVIM-7-F218Y was further dialyzed in buffer D overnight before being purified using ion-exchange purification on a 5-ml HiTrap Q column (GE Healthcare) equilibrated in buffer D. The mutant was eluted across a gradient of 0 to 100% buffer G (50 mM HEPES [pH 7.2], 100 μM $ZnCl_2$, 1 M NaCl). Finally, all proteins were stored at 4°C in buffer C after concentration to 12 to 18 mg/ml.

Generally, purified proteins were at a level of more than 95% purity as judged by SDS-PAGE analysis. The identity of all recombinant proteins was confirmed by tandem mass spectrometry (MS/MS) analysis. Typical yields from 1 liter of cell culture were about 0.8 mg of protein for the periplasmic VIM-7 purification and about 3.5 to 5.0 mg of protein from the TEV protease-cleaved tVIM-7 constructs.

Enzyme kinetics for VIM-7, tVIM-7, tVIM-7-D120A, tVIM-7-F218Y, and tVIM-7-H224Y. The steady-state kinetic measurements were performed at 25°C in UV-transparent 96-well plates (Corning) using SpectraMax 190 (Molecular Devices) for VIM-7 and tVIM-7-D120A or the $M2^e$ spectrophotometer (Molecular Devices) for tVIM-7, tVIM-7-F218Y, and tVIM-7-H224Y in assay buffer H (50 mM HEPES [pH 7.2], 100 μM $ZnCl_2$, 1.0 mg/ml bovine serum albumin). The final protein concentration in the enzyme assay was 1 to 50 nM, and it was up to 100 nM for tVIM-7-D120A. K_m (μM) and k_{cat} (s^{-1}) were determined from plots of the initial velocity of hydrolysis against substrate concentration. For benzylpenicillin and ampicillin, the K_m was determined as the K_i by measuring inhibition of hydrolysis of the reporter substrate nitrocefin across a range of substrate and nitrocefin concentrations, using half-area 96-well plates (Corning). K_i values were determined by a global (shared-parameter) fit of these multiple data sets to a competitive inhibition model. All kinetic data were fitted by nonlinear regression as implemented in the GraphPad Prism software (GraphPad).

Crystallization, data collection, structure determination, and docking. tVIM-7 and the respective mutants tVIM-7-D120A, VIM-7-F218Y, t-VIM-7H224Y were crystallized by the hanging-drop method in reservoir volumes of 60 to 500 μl and by mixing equal volumes of protein and reservoir to a final drop size of 1.0 to 2.0 μl under different conditions as reported earlier (16). The protein concentrations were 13 mg/ml for tVIM-7, 18 mg/ml for tVIM-7-D120A, 12 mg/ml for VIM-7-F218Y, and 17 mg/ml for tVIM-7-H224Y.

tVIM-7 was crystallized at 4°C from reservoirs containing 19% polyethylene glycol 3350 (PEG 3350), 0.1 M calcium acetate, 0.1 M succinate (pH 7.0), and cryo-protected in cryo1 (25% PEG 3350, 20% glycerol, and 0.1 M succinate [pH 7.0]). tVIM-7-D120A was crystallized at 22°C from 26% PEG 5000 monomethyl ether (PEG 5K MME) and 0.1 M sodium citrate (pH 5.5), and cryo-protected in cryo2 (20% PEG 2K MME, 25% glycerol, 0.1 M cacodylate [pH 5.0]). VIM-7-F218Y was crystallized at 22°C from a mixture of 24% PEG 5K MME, 10% glycerol, and 0.1 M sodium citrate buffer (pH 8.0) and then transferred to cryo1. tVIM-7-H224Y had reservoir solutions with 25% PEG 3350, 0.1 M Bis-Tris (pH 5.5) and 0.2 M NaCl, and was cryoprotected in cryo3 (32% PEG 5K MME, 5% glycerol, 0.1 M succinate buffer [pH 7.0]). All crystals were flash-cooled in liquid nitrogen.

The X-ray data were collected at Beamlines I911-3 at the Max laboratory in Lund, Sweden, and at BL14.1 at BESSY, Berlin, Germany (Table 2). The phase problem was solved by molecular replacement starting from VIM-7 (Protein Data Bank [PDB] no. 2Y8B), and the structures were refined in Phenix (38) or REFMAC5 (39), with manual rebuilding done in WinCoot (40). Ceftazidime was docked into the tVIM-7, tVIM-7-H224Y, and VIM-7-F218Y structures, starting from the previously reported

TABLE 2 X-ray data collection and crystallographic refinement statistics for the new VIM-7 structures

Parameter	Result for construct[a]: TEV site tVIM-7	tVIM-7-D120A	tVIM-7-H224Y	Leader sequence VIM-7-F218Y
Data collection				
X-ray source	BESSY, BL14.1	BESSY, BL14.1	MAX-lab, I911-3	BESSY, BL14.1
Space group	$P4_3$	$P4_3$	$P4_3$	$P4_3$
Unit cell dimensions, Å	$a = b = 69.98$, $c = 47.53$	$a = b = 69.76$, $c = 47.29$	$a = b = 70.23$, $c = 47.03$	$a = b = 69.95$, $c = 46.94$
Resolution, Å	30-1.25 (1.32-1.25)	40-1.80 (1.90-1.80)	30-1.40 (1.48-1.40)	50-1.70 (1.79-1.70)
Wavelength, Å	0.91841	0.91841	1.0000	0.91841
No. of unique reflections	61,189	21,271 (3,100)	43,649 (5,673)	25,160 (14,553)
Multiplicity	2.9 (1.6)	4.2 (4.1)	3.5 (2.0)	4.0 (4.0)
Completeness, %	96.4 (78.2)	100.0 (100.0)	96.6 (86.8)	100.0 (100.0)
Mean ($\langle I\rangle/\sigma\langle I\rangle$)	14.1 (2.0)	13.2 (2.6)	9.1 (3.1)	16.3 (2.6)
R-sym, %[b]	3.8 (42.3)	7.7 (53.9)	6.6 (16.5)	5.9 (56.0)
Wilson B-factor, Å^2	8.9	18.2	12.8	16.3
Refinement				
PDB entry no.	4D1T	4D1U	4D1W	4D1V
Resolution, Å	25-1.25	25-1.80	25-1.40	25-1.7
R-factor (all reflections), %	13.07	16.06	11.78	15.93
R_{free}, %[c]	14.83	20.75	15.64	19.65
No. of:				
Atoms (no H)	2,120	1,876	2,020	1,955
Water molecules	280	152	258	241
Other molecules	2 Zn^{2+}	1 Zn^{2+}	2 Zn^{2+}	2 Zn^{2+}
RMSD:				
Bond lengths, Å	0.009	0.010	0.014	0.007
Bond angles, °	1.39	1.30	1.52	1.14
Avg B-factor, Å^2				
All atoms	14.5	19.3	18.4	25.4
Protein	12.7	18.5	16.4	24.1
Solvent (Zn^{2+})	26.6 (7.3)	28.3 (13.1)	31.8 (17.0)	34.5 (25.3)
Ramachandran plot, %				
Favored	96.9	98.0	94.7	95.7
Allowed	2.2	1.1	3.9	3.3
Outliers	0.9	0.9	1.4	1.0
Occupancy for Zn1/Zn2	1.0/0.90	1.0/0.0	0.9/0.4	0.9/0.5

[a] Values in parentheses are for the highest-resolution shell.
[b] *R*-sym = $\{[\Sigma_h\Sigma_i \mid I_i(h) - \langle I(h)\rangle|]/[\Sigma_h\Sigma_I I(h)]\}$, where $I_i(h)$ is the *i*th measurement of reflection *h* and $\langle I(h)\rangle$ is the weighted mean of all measurements of *h*.
[c] Five percent of the reflections were used in the R_{free} calculations.

docked conformations for this substrate in VIM-7 (3 different conformations) and in VIM-2 (3 different conformations) (16).

Fluorescence-based protein thermal stability assay. The thermal stability of all VIM-7 variants was determined by a fluorescence-based protein thermal stability assay (41) in a MJ minicycler (Bio-Rad) across a temperature gradient of 10 to 70°C with a heating rate of 1° min^{-1}. The total assay volume of 25 μl included 7 to 9 μM protein, 90× SYPRO orange solution (Sigma-Aldrich), and 50 mM HEPES (pH 7.5). Thermostability was also investigated in the presence of 400 μM $ZnCl_2$ or 1 mM EDTA. The excitation and emission wavelengths of SYPRO orange are 470 nm and 570 nm, respectively. All experiments were performed in duplicate, and the melting temperatures (T_m) were determined as the inflection point of the melting transition found from the first derivative.

Protein structure accession numbers. Coordinates and structure factors have been deposited in the Protein Data Bank under accession no. 4D1T (tVIM-7), 4D1U (tVIM-7-D120A), 4D1V (VIM-7-F218Y), and 4D1W (tVIM-7-H224Y).

RESULTS AND DISCUSSION

Analysis of different VIM-7 constructs. In this study, two different VIM-7 constructs were utilized. One construct encoding the recombinant version of the native VIM-7 (previously described by Borra et al. [16]) and one construct encoding residues Ala25 to Glu300 in VIM-7 where the leader sequence and eight additional residues were replaced with a TEV protease-cleavable N-terminal hexahistidine tag (tVIM-7). The tVIM-7 construct was made due to a low recovery of recombinant VIM-7 after periplasmic purification and to improve purification yields by cytoplasmic expression. Through comparison of the enzymatic activities of the two

TABLE 3 Steady-state kinetic results for tVIM-7, tVIM-7-F218Y, and tVIM-7-H224Y

Compound	tVIM-7			tVIM-7-F218Y			tVIM-7-H224Y		
	K_m (μM)	k_{cat} (s^{-1})	k_{cat}/K_m ($s^{-1} \cdot \mu M^{-1}$)	K_m (μM)	k_{cat} (s^{-1})	k_{cat}/K_m ($s^{-1} \cdot \mu M^{-1}$)	K_m (μM)	k_{cat} (s^{-1})	k_{cat}/K_m ($s^{-1} \cdot \mu M^{-1}$)
Penicillins									
Benzylpenicillin[a]	23 ± 3	59 ± 7	2.5	2.2 ± 0.6	198 ± 14	89	29.8 ± 3.0	144 ± 12	4.83
Ampicillin[a]	23.3 ± 1.7	17.6 ± 1.1	0.76	0.78 ± 0.26	17 ± 5	20	37 ± 11	170 ± 4	4.63
Cephalosporins									
Cefepime	179 ± 14	0.450 ± 0.023	0.0025	79 ± 9	1.66 ± 0.08	0.02	108 ± 20	4.4 ± 0.3	0.041
Ceftazidime	61 ± 19	0.120 ± 0.007	0.0020	62 ± 20	1.4 ± 0.3	0.02	30 ± 6	0.39 ± 0.02	0.013
Cefoxitin	20 ± 4	0.64 ± 0.03	0.032	12.7 ± 0.8	3.50 ± 0.08	0.278	15.5 ± 2.0	3.9 ± 0.1	0.25
Cefuroxime	12.9 ± 2.5	4.57 ± 0.05	0.35	6.3 ± 0.6	22.5 ± 0.5	3.6	13.7 ± 2.1	5.5 ± 0.2	0.40
Carbapenems									
Ertapenem	18.9 ± 2.2	12.810 ± 0.013	0.68	6.4 ± 0.3	6.06 ± 0.07	0.95	14.0 ± 1.1	8.95 ± 0.13	0.64
Imipenem	29 ± 10	7.71 ± 0.17	0.27	9.3 ± 0.6	24.7 ± 0.3	2.7	27.8 ± 2.4	50.0 ± 0.9	1.80
Meropenem	20.0 ± 1.6	25.580 ± 0.026	1.28	15.9 ± 0.6	11.7 ± 0.1	0.74	25.3 ± 2.7	23.9 ± 0.5	0.94

[a] The K_m values were measured as inhibition constants (K_i) in a competitive model using nitrocefin as the reporter substrate.

recombinant variants, we found that the catalytic efficiency (k_{cat}/K_m) was higher for VIM-7 than for tVIM-7 (2 to 84 times) for most substrates investigated, except ertapenem and meropenem (see Table S1 in the supplemental material). The differences were most profound for penicillins. The increased catalytic efficiency was due to both improved binding (lower K_m) and higher turnover (k_{cat}) (Table 3; see Table S1 in the supplemental material). Due to the differences in the constructs, the N termini of VIM-7 and tVIM-7 will be different. According to the SignalP signal peptide prediction server (http://www.cbs.dtu.dk/services/SignalP/), cleavage of the leader sequence is likely to occur between amino acids Ala16 and Val17 in VIM-7. Structural analysis confirmed the presence of residues Glu30 to Thr292 in VIM-7 (16); however, any remaining N-terminal residues were disordered in the X-ray structure. Following TEV protease cleavage of tVIM-7, a glycine and an alanine residue remain at the N terminus of the recombinant protein, which are not present in the wild-type sequence (corresponding to Gly23-Ala24-Ala25). In order to investigate these differences further, the structure of the recombinant tVIM-7 was solved by X-ray crystallography to 1.25 Å and compared to three VIM-7 structures (PDB entries 2Y8A, 2Y8B, and 2Y87) (16). The first ordered amino acid residue in the tVIM-7 structure is Gly29 (indicated in Fig. 1a), which is similar to what was observed for VIM-7 (16). How the differences in the N termini of the two recombinant proteins VIM-7 and tVIM-7 affect the catalytic activity have not been elucidated.

Generally, the protein backbone fits well into the observed electron density of tVIM-7, including residues Gly29 to Lys293, which represent a sequence 2 to 3 residues longer than was observed in the VIM-7 structures. The root mean square deviations (RMSDs) for the CA atoms of tVIM-7 were 0.50, 0.15, and 0.48 Å, compared to PDB 2Y8A (VIM-7-S; with an S atom between the two zinc ions), 2Y8B (VIM-7-Ox; with an oxidized Cys221), and 2Y87 (VIM-7; native), respectively. There are some conformational differences in the L3 loop (residues 223 to 240), but these were also found between the three VIM-7 structures (16) and are most likely due to the flexibility of the loop. Since the zinc-coordinating residues (Fig. 2a) and the second shell residues interacting with the active site (e.g., Arg228) are similar, the structural differences in the backbone cannot explain the observed higher catalytic efficiency for VIM-7 than that for tVIM-7 (Table 3). The observed enzymatic differences could not be related to thermal stability, since the observed melting temperature (T_m) of VIM-7 (57.4°C) was slightly higher than that of tVIM-7 (55.3°C) (Fig. 3).

Mutation of D120A affects zinc binding and catalysis. The role of the zinc ions (Zn1 and Zn2) in MBLs is complex and controversial (17). Residue Asp120 in the VIM-7 structure was found bound to Zn2 and a hydroxyl ion (W1) (16) and consequently was important for catalysis as shown for other MBLs such as CcrA, L1, IMP-1, and BcII (22–24, 26, 42). To investigate the importance of this residue, the tVIM-7-D120A mutant was created. The enzyme kinetics showed that the tVIM-7-D120A mutant was inactive toward nitrocefin and ertapenem, even at very high enzyme concentrations (100 nM) (data not shown). Determination of the crystal structure of tVIM-7-D120A to a 1.9-Å resolution (Table 2) and refinement with respect to the occupancy of the Zn2 ion showed that Zn2 converged at an occupancy of 0.33 with interactions with Cys221 SG and His263 NE2. This indicates that the Zn2 site was occupied by a water molecule (H_2O) with 10 electrons, since 30 electrons in zinc multiplied by an occupancy of 0.33 is 10 electrons, and that tVIM-7D120A is then a monozinc variant (Fig. 2b). Previous reports have also shown that Asp120 is an important residue for Zn coordination in the VIM family of enzymes and therefore is essential for the catalytic activity (22–24, 26, 42). One explanation for the tVIM-7-D120A mutant being inactive is that the observed W1 water molecule is not a good nucleophile for catalysis, in contrast to a hydroxyl ion as previously suggested (17, 21, 43). In addition, the tVIM7-D120A mutant was found to be less stable (48.5°C) than the wild-type tVIM-7 (Table 4). However, the observed thermal shift observed for the tVIM-7-D120A mutant indicates that the structural integrity of the protein is intact (Fig. 3). The thermally induced melting seemed to start at a lower temperature, observed from a less steep unfolding slope. We speculate on whether the low stability is related to the fact that the mutant binds only one zinc ion, not two as in the wild type, contributing to a local destabilization of the active-site region. Interestingly, the addition of zinc to the buffer in a relative molar ratio of approximately 50:1 decreased the thermal stability of all our

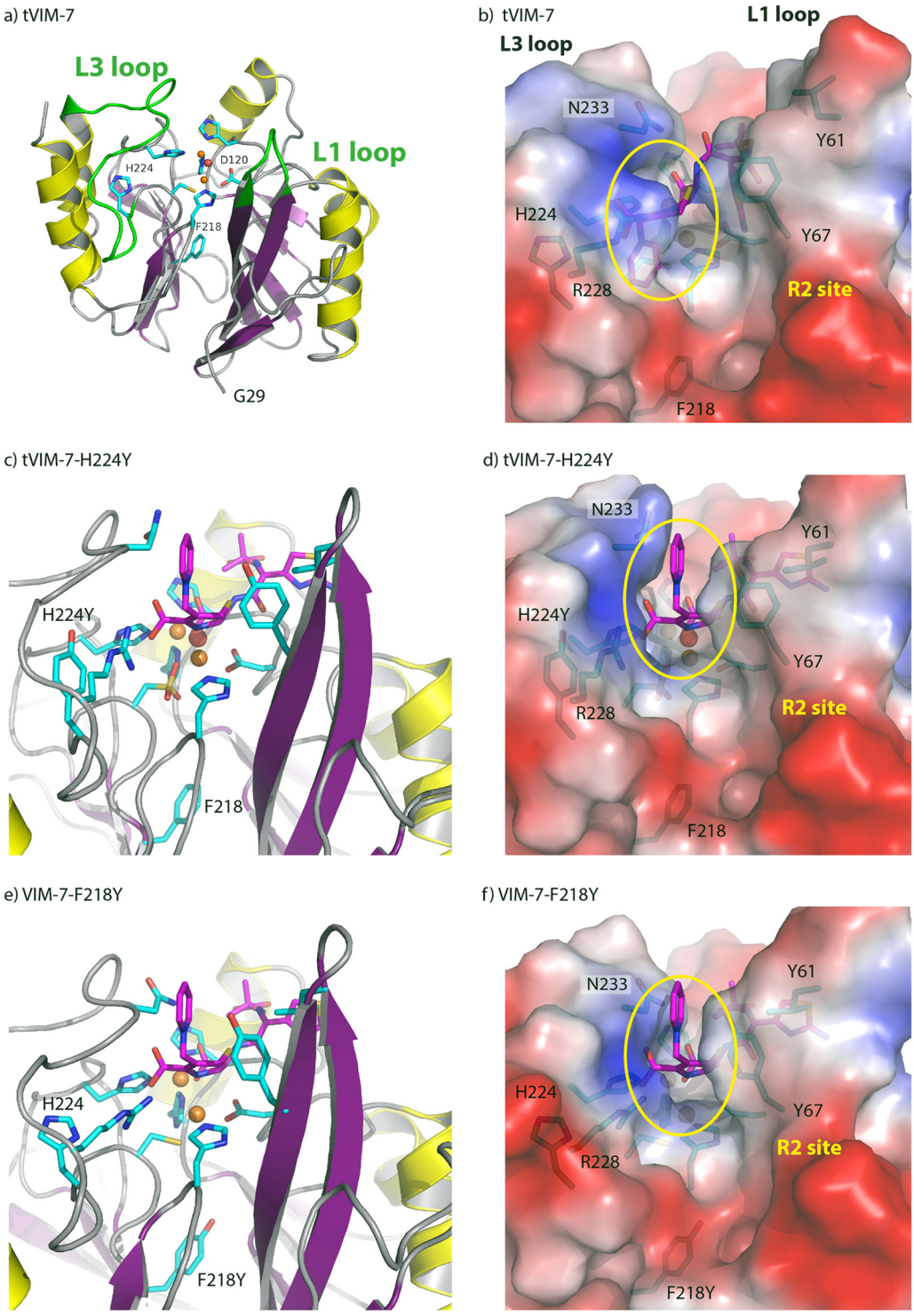

FIG 1 VIM-7 structures. Shown are ribbon diagrams of the tVIM-7 wild type with the L1 (residues 60 to 66) and L3 (residues 223 to 240) loops in green (a), the tVIM-7-H224Y mutant (c), and the VIM-7-F218Y mutant (e) structures, with the corresponding calculated electrostatic surface potentials shown in panels b, c, and d. Ceftazidime (magenta) with a cyclic positively charged R2 group was docked and is shown in panels b to f.

recombinant proteins (Table 4). Thus, we observed a negative effect from zinc on the overall stability when a surplus of zinc is added. This could indicate that there are nonspecific zinc-binding sites outside of the active-site region that contribute to destabilizing the protein. Previously, it was reported that for VIM-4, the addition of zinc also decreased the stability from 58.5°C for the wild type to 44.4°C and 56.6°C for the two unfolding transitions observed with zinc (20). Not surprisingly, the addition of the zinc

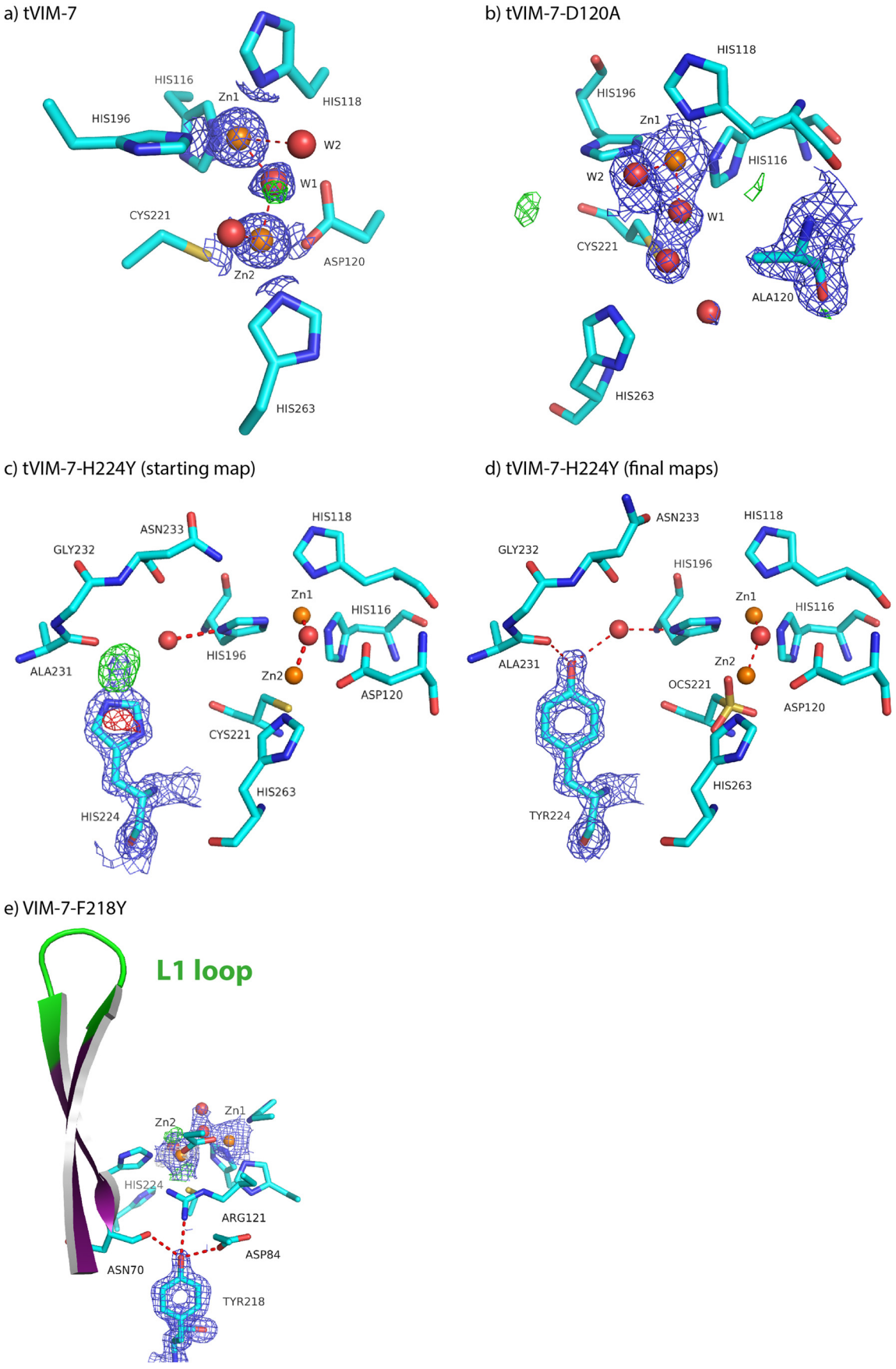

FIG 2 Electron density maps from the new structures showing close-ups of the mutated residues and active-site regions. Shown are $2F_o$-F_c maps for tVIM-7 (1.8 σ) (a) and tVIM-7-D120A (1.3 σ) (b) and the starting (c) and final (d) electron density maps of residue 224 in tVIM-7-H224Y (1.6 σ) and VIM-7-F218Y (1.8 σ) (e). Positive (+4σ, green) and negative (−4σ, red) difference electron density is contoured in all panels. Adjacent and interacting residues are also displayed.

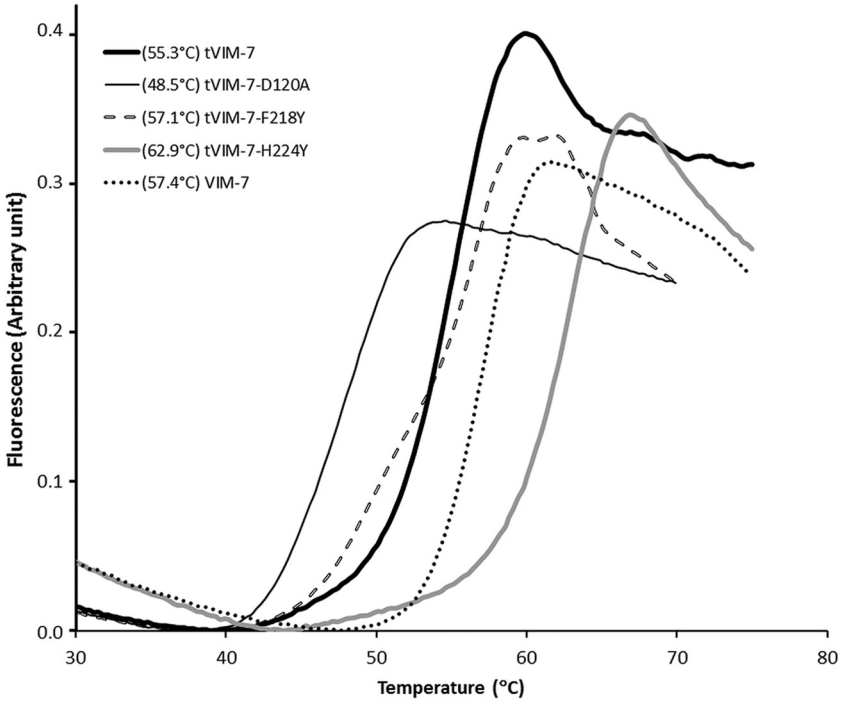

FIG 3 Thermal unfolding curves from ThermoFluor experiments. The fluorescence signals display tVIM-7 (black solid line), tVIM-7-D120A (thin black line), tVIM-7-F218Y (dashed line), tVIM-7-H224Y (thick gray line), and VIM-7 (dotted line), with the observed T_ms in parentheses.

chelator EDTA did not give any inflection points for any of the recombinant VIM-7 proteins. Again, this emphasizes the importance of zinc binding for correct folding of the VIM enzymes.

Overall, the structure of the tVIM-7-D120A mutant resembled that of tVIM-7 with an RMSD of 0.63 Å. Minor differences were observed in the L1 loop (residues 60 to 66) of the mutant, resulting in a more closed position of the loop, and His263 was rotated slightly, with its NE2 atom moved 1.3 Å relative to tVIM-7. The Zn1 position has five ligands, namely, His116, His118, His196, W1, and an additional water molecule, W2 (Fig. 2b), similar to the VIM-7-Ox (PDB no. 2Y8B) structure (16).

The reduced activity of VIM-7 compared to that of VIM-2 could partly be explained by the lack of a hydrogen bond network around residue 218. Previously, we reported that the lack of the two hydrogen bond clusters involving residues 224 or 218, could be a determinant of the increased flexibility and reduced activity of VIM-7 compared to VIM-2 (16). To study the involvement of these residues and the SAR in VIM-7, we mutated these residues to tyrosine residues as they appear in VIM-2. For residue 218, the assumptions were based on studies of the IMP-1-F218Y mutant, which showed increased catalytic efficiency compared to the wild type through improved movements of the lid that covers the active site (28, 29). The lid includes the two anti-parallel β-strands connected by the L1 loop. Compared to the VIM-7 structure, three additional hydrogen bonds were observed in the VIM-7-F218Y structure linking together different secondary elements, making the structure more rigid. The OH atom of Tyr218 was hydrogen bonded to Asn70 O, Asp84 OD2, and Arg121 NH1 (Fig. 2e). This hydrogen bond network is also observed in VIM-2 and VIM-4 (16, 19, 20) and most likely is also found in tVIM-7-F218Y since the VIM-7-F218Y structure is very similar to that of tVIM-7, with an RMSD of 0.5 Å for all CA atoms.

TABLE 4 Apparent average melting temperatures of VIM-7 and mutants as found by ThermoFluor assays[a]

Protein	T_m (°C) for:		ΔT_m (°C)
	pH 7.5	pH 7.5 + $ZnCl_2$	
tVIM-7	55.3 ± 0.2	48.4 ± 0.2	−6.9
tVIM-7-D120A	48.5 ± 0.1	46.1 ± 0.1	−2.4
tVIM-7-H224Y	62.9 ± 0.1	60.2 ± 0.1	−2.7
tVIM-7-F218Y	57.1 ± 0.8	57.0 ± 0.6	−0.1
VIM-7	57.4 ± 0.2	53.8 ± 0.2	−3.6

[a] The assays were performed in 50 mM HEPES (pH 7.5) with 400 μM $ZnCl_2$ or 1 mM EDTA (data not shown). The experiments were performed in duplicate.

For the IMP-1-F218Y mutant, increased activity was observed (28, 29), and this was also found for our tVIM-7-F218Y experiments (Table 3). The tVIM-7-F218Y mutant had better penicillin and ampicillin binding properties in terms of lower K_m values, and the catalytic efficiencies against the tested cephalosporins were 8 (cefepime), 12 (ceftazidime), 9 (cefoxitin), and 10 (cefuroxime) times higher than those for the tVIM-7 wild type. This was mainly due to higher turnover (k_{cat}). For the carbapenems, the activities were similar for meropenem and ertapenem but 10 times higher for tVIM-7-F218Y toward imipenem. Consequently, the observed increase in catalytic efficiently of the tVIM-7-F218Y mutant is due to both tighter binding and higher turnover, depending on the substrate.

The thermostability is somewhat higher for the tVIM-7-F218Y mutant (T_m, 57.1°C) compared to tVIM-7 (55.3°C) (Table 4). Both the enhanced activity and stability are most likely due to the three additional hydrogen bonds from F218Y OH. Phe218 in the native VIM-7 is not involved in this hydrogen-bonding cluster, thus indicating that the reduced activity of VIM-7 compared to

that of VIM-2 could be related to the absence of these hydrogen bonds. The conformations of the lid with two anti-parallel β-strands connected by the L1 loop (residues 60 to 66) are very similar in the new crystal structures of tVIM-7 and VIM-7-F218Y, so a big lid movement or lid pulldown effect is not observed to explain the difference. Still a more tightly bound lower plateau in the active site seems favorable in the F218Y mutant.

The H224Y mutation in the L3 loop demonstrates the importance of residue 224 in the catalysis. Previously, we have observed lower catalytic efficiency of VIM-7 for cephalosporins with bulky or charged C-3 substituents (R2 groups) compared to VIM-2 (15). Based on the VIM-7 crystal structure, we hypothesized that His224 and Phe218 were involved in the observed reduced catalytic efficiency (16). Furthermore, the L3 loop, consisting of residues 223 to 240, has been shown to play a role in B1 MBLs (27, 31, 44). Residue 224 was found to be a lysine in many B1 MBLs (33), and the positively charged side chain is thought to be important for both binding and positioning of substrate (45) to various degrees (33, 46, 47). In VIM-7, His224 in the L3 loop protrudes into the R2 antibiotic binding site, contributing with a positive charge (16). By mutating this residue to tyrosine (as in VIM-2), we found the enzyme activity of the tVIM-7-H224Y mutant to be higher than that of wild-type tVIM-7 against all substrates, with the exception of ertapenem and meropenem (Table 3). The highest increase in activity was observed toward the three cephalosporins cefepime, cefoxitin, and ceftazidime, where the tVIM-7-H224Y mutant showed 16, 8, and 7 times higher catalytic efficiencies, respectively (Table 3), compared to tVIM-7. Both cefepime and ceftazidime have positively charged cyclic R2 groups and were found to have a higher turnover by the tVIM-7-H224Y mutant than to the tVIM-7 wild type. The carbapenemase activities of the mutant compared to those of the wild type were similar for two of the substrates, but the activity was 7 times higher toward imipenem, possibly due to the positively charged R2 group of imipenem.

Structurally, tVIM-7-H224Y was found to be very similar to the tVIM-7 structure, with an RMSD of 0.23 Å (for CA atoms). In the tVIM-7-H224Y crystal structure, the introduced tyrosine residue at 224 formed one additional hydrogen bond to the main-chain oxygen of Ala231 and another water-intermediated hydrogen bond to the Zn1 ligand H196 ND1 (Fig. 2c and d). Two additional hydrogen bonds close to the active site may have strong effects with respect to activity. Furthermore, Arg228 was found almost parallel to the aromatic phenyl ring of Tyr224, resulting in an open U-shaped R2 binding site (Fig. 1d). This was different from tVIM-7, where Arg228 blocked and confined the size of the R2 site (Fig. 1b). Compared to VIM-2, the water-mediated hydrogen bond is the same, but in VIM-2, Tyr224 OH is bound to Gly232 N and not Ala231 O as in tVIM-7-H224Y. The side chain of Asn233 was partly disordered in tVIM-7-H224Y. The ThermoFluor experiments showed that the introduction of these interactions in tVIM-7-H224Y increased the stability (T_m, 62.9°C) compared to that of the tVIM-7 wild-type enzyme (T_m, 55.4°C) (Table 4).

Comparative studies between VIM-1 (His224 and Ser228) and VIM-13 (Leu224 and Arg228) have also shown that the residue composition in the L3 loop influences the activity particularly against substrates such as ceftazidime and cefepime (31). This supports our enzyme kinetics and the crystal structure analysis of the tVIM-7-H224Y mutant. Our data underline the importance of position 224 in the L3 loop with respect to catalytic efficiency. The tyrosine in position 224 of VIM-2 may be an important residue determinant for its high catalytic activity.

Docking of ceftazidime in the VIM-7 wild type and mutants. In order to further analyze the SAR of the mutants and the lower activity of VIM-7 toward cephalosporins with a bulky, positively charged R2 group, ceftazidime was docked into the structures of tVIM-7 and the two mutants, tVIM-7-H224Y and VIM-7-F218Y. In line with the previously reported VIM-7 structure (16), the cyclic R2 group of ceftazidime was adjacent to His224 and buried below Arg228 in wild-type tVIM-7 (Fig. 1b). In contrast, this substrate conformation does not fit into either of the tVIM-7-H224Y or VIM-7-F218Y mutant structures. We hypothesize that a stacking between Tyr67 in the L1 loop of VIM-7 and the positively charged R2 ring of ceftazidime is more likely to occur for this particular substrate. Arg228 is the major contributor to the alternative ceftazidime conformation in both mutants, since this residue partly overlaps the ceftazidime conformation in tVIM-7 (Fig. 1b to f).

Conclusions. As previously shown for other MBLs (22–24, 26, 42), the aspartic acid at position 120 in VIM-7 was found to be important for metal coordination and was essential for enzyme catalysis, resulting in a inactive enzyme. By structural analysis, we found that the VIM-7-F218Y mutant contained more hydrogen bonds than the tVIM-7 wild type, indicating a higher thermal stability. This was also confirmed by a slightly higher melting temperature and a higher enzyme activity. Based on our data, we conclude that the reduced activity of VIM-7, compared to VIM-2, can be attributed to the absence of the hydrogen bond cluster around residue 218 alone and that residue 218 seems to be an important residue determinant for activity of the VIM family of enzymes as in IMP enzymes (28, 29). In addition, interactions found between Tyr224 and Ala231 in the tVIM-7-H224Y structure resulted in a stabilization of the L3 loop and an increase in melting temperature, reflecting a more thermostable enzyme, and could explain the increased activity of the tVIM-7-H224Y mutant. We therefore conclude that residue 224 in the L3 loop is an important residue determinant for both stability and enzyme activity for the VIM family of metallo-β-lactamases. During catalysis, the L3 loop of VIM-7 is most likely flexible in a fashion similar to that found for the L3 loop of GIM-1 (27). Still, the interplay between residues 224 and 228 in the L3 loop and 67 in the L1 loop also seems important for activity. Overall, the analysis of both the F218Y and H224Y mutants indicates that not only the local rearrangements but also the positions of these residues in the folded enzyme structure are important for the enzyme properties.

ACKNOWLEDGMENTS

We are grateful to Trine Josefine Olsen Carlsen for excellent help with cloning, protein expression, purification, and crystallization and Pardha Saradhi Borra for making the VIM-7-F218Y mutant. Provision of beam time at BL14.1, BESSY, and at I911-3, Max Lab II, Lund, Sweden, is gratefully acknowledged. Assistance with data collection by Ronny Helland is highly valued.

The Norwegian Structural Biology Centre (NorStruct) was supported by the National Functional Genomics Program (FUGE) of the Research Council of Norway. Additional funding from the Northern Norway Regional Health Authority, Tromsø Research Foundation, and Research Council of Norway (FRIMEDBIO project number 213808) is also acknowledged.

H.-K.S.L., S.S., K.S.W.E., M.S.L., G.E.K.B., I.L., and Ø.S. conceived

and designed the experiments. S.S., K.S.W.E., and H.-K.S.L. performed the experiments. H.-K.S.L., S.S., K.S.W.E., M.S.L., G.E.K.B., Ø.S., and I.L. analyzed the data. H.-K.S.L., Ø.S., and G.E.K.B. wrote the manuscript.

REFERENCES

1. **Cornaglia G, Giamarellou H, Rossolini GM.** 2011. Metallo-β-lactamases: a last frontier for β-lactams? Lancet Infect. Dis. **11:**381–393. http://dx.doi.org/10.1016/S1473-3099(11)70056-1.
2. **Papp-Wallace KM, Endimiani A, Taracila MA, Bonomo RA.** 2011. Carbapenems: past, present, and future. Antimicrob. Agents Chemother. **55:**4943–4960. http://dx.doi.org/10.1128/AAC.00296-11.
3. **Patel G, Bonomo RA.** 2013. "Stormy waters ahead": global emergence of carbapenemases. Front. Microbiol. **4:**48. http://dx.doi.org/10.3389/fmicb.2013.00048.
4. **Bush K, Fisher JF.** 2011. Epidemiological expansion, structural studies, and clinical challenges of new β-lactamases from gram-negative bacteria. Annu. Rev. Microbiol. **65:**455–478. http://dx.doi.org/10.1146/annurev-micro-090110-102911.
5. **Walsh TR.** 2010. Emerging carbapenemases: a global perspective. Int. J. Antimicrob. Agents **36**(Suppl 3)**:**S8–S14. http://dx.doi.org/10.1016/S0924-8579(10)70004-2.
6. **Walsh TR, Toleman MA, Poirel L, Nordmann P.** 2005. Metallo-β-lactamases: the quiet before the storm? Clin. Microbiol. Rev. **18:**306–325. http://dx.doi.org/10.1128/CMR.18.2.306-325.2005.
7. **Bush K.** 2013. Proliferation and significance of clinically relevant β-lactamases. Ann. N. Y. Acad. Sci. **1277:**84–90. http://dx.doi.org/10.1111/nyas.12023.
8. **Nordmann P, Poirel L, Walsh TR, Livermore DM.** 2011. The emerging NDM carbapenemases. Trends Microbiol. **19:**588–595. http://dx.doi.org/10.1016/j.tim.2011.09.005.
9. **Queenan AM, Bush K.** 2007. Carbapenemases: the versatile β-lactamases. Clin. Microbiol. Rev. **20:**440–458. http://dx.doi.org/10.1128/CMR.00001-07.
10. **Picão RC, Poirel L, Gales AC, Nordmann P.** 2009. Diversity of β-lactamases produced by ceftazidime-resistant *Pseudomonas aeruginosa* isolates causing bloodstream infections in Brazil. Antimicrob. Agents Chemother. **53:**3908–3913. http://dx.doi.org/10.1128/AAC.00453-09.
11. **Bush K, Jacoby GA.** 2010. Updated functional classification of β-lactamases. Antimicrob. Agents Chemother. **54:**969–976. http://dx.doi.org/10.1128/AAC.01009-09.
12. **Bush K.** 2013. The ABCD's of β-lactamase nomenclature. J. Infect. Chemother. **19:**549–559. http://dx.doi.org/10.1007/s10156-013-0640-7.
13. **Rodriguez-Martinez JM, Nordmann P, Fortineau N, Poirel L.** 2010. VIM-19, a metallo-β-lactamase with increased carbapenemase activity from *Escherichia coli* and *Klebsiella pneumoniae*. Antimicrob. Agents Chemother. **54:**471–476. http://dx.doi.org/10.1128/AAC.00458-09.
14. **Toleman MA, Rolston K, Jones RN, Walsh TR.** 2004. bla_{VIM-7}, an evolutionarily distinct metallo-β-lactamase gene in a *Pseudomonas aeruginosa* isolate from the United States. Antimicrob. Agents Chemother. **48:**329–332. http://dx.doi.org/10.1128/AAC.48.1.329-332.2004.
15. **Samuelsen Ø, Castanheira M, Walsh TR, Spencer J.** 2008. Kinetic characterization of VIM-7, a divergent member of the VIM metallo-β-lactamase family. Antimicrob. Agents Chemother. **52:**2905–2908. http://dx.doi.org/10.1128/AAC.00166-08.
16. **Borra PS, Leiros H-KS, Ahmad R, Spencer J, Leiros I, Walsh TR, Sundsfjord A, Samuelsen Ø.** 2011. Structural and computational investigations of VIM-7: insights into the substrate specificity of VIM metallo-β-lactamases. J. Mol. Biol. **411:**174–189. http://dx.doi.org/10.1016/j.jmb.2011.05.035.
17. **Page MI, Badarau A.** 2008. The mechanisms of catalysis by metallo β-lactamases. Bioinorg Chem. Appl. **2008:**576297. http://dx.doi.org/10.1155/2008/576297.
18. **Gonzalez JM, Meini MR, Tomatis PE, Medrano Martin FJ, Cricco JA, Vila AJ.** 2012. Metallo-β-lactamases withstand low Zn(II) conditions by tuning metal-ligand interactions. Nat. Chem. Biol. **8:**698–700. http://dx.doi.org/10.1038/nchembio.1005.
19. **Garcia-Saez I, Docquier JD, Rossolini GM, Dideberg O.** 2008. The three-dimensional structure of VIM-2, a Zn-β-lactamase from *Pseudomonas aeruginosa* in its reduced and oxidised form. J. Mol. Biol. **375:**604–611. http://dx.doi.org/10.1016/j.jmb.2007.11.012.
20. **Lassaux P, Traore DA, Loisel E, Favier A, Docquier JD, Sohier JS, Laurent C, Bebrone C, Frere JM, Ferrer JL, Galleni M.** 2011. Biochemical and structural characterization of the subclass B1 metallo-β-lactamase VIM-4. Antimicrob. Agents Chemother. **55:**1248–1255. http://dx.doi.org/10.1128/AAC.01486-09.
21. **Palzkill T.** 2013. Metallo-β-lactamase structure and function. Ann. N. Y. Acad. Sci. **1277:**91–104. http://dx.doi.org/10.1111/j.1749-6632.2012.06796.x.
22. **Crisp J, Conners R, Garrity JD, Carenbauer AL, Crowder MW, Spencer J.** 2007. Structural basis for the role of Asp-120 in metallo-β-lactamases. Biochemistry **46:**10664–10674. http://dx.doi.org/10.1021/bi700707u.
23. **Garrity JD, Carenbauer AL, Herron LR, Crowder MW.** 2004. Metal binding Asp-120 in metallo-β-lactamase L1 from *Stenotrophomonas maltophilia* plays a crucial role in catalysis. J. Biol. Chem. **279:**920–927. http://dx.doi.org/10.1074/jbc.M309852200.
24. **Yamaguchi Y, Kuroki T, Yasuzawa H, Higashi T, Jin W, Kawanami A, Yamagata Y, Arakawa Y, Goto M, Kurosaki H.** 2005. Probing the role of Asp-120(81) of metallo-β-lactamase (IMP-1) by site-directed mutagenesis, kinetic studies, and X-ray crystallography. J. Biol. Chem. **280:**20824–20832. http://dx.doi.org/10.1074/jbc.M414314200.
25. **Bebrone C, Anne C, Kerff F, Garau G, De Vriendt K, Lantin R, Devreese B, Van Beeumen J, Dideberg O, Frere JM, Galleni M.** 2008. Mutational analysis of the zinc- and substrate-binding sites in the CphA metallo-β-lactamase from *Aeromonas hydrophila*. Biochem. J. **414:**151–159. http://dx.doi.org/10.1042/BJ20080375.
26. **de Seny D, Prosperi-Meys C, Bebrone C, Rossolini GM, Page MI, Noel P, Frere JM, Galleni M.** 2002. Mutational analysis of the two zinc-binding sites of the *Bacillus cereus* 569/H/9 metallo-β-lactamase. Biochem. J. **363:**687–696. http://dx.doi.org/10.1042/0264-6021:3630687.
27. **Borra PS, Samuelsen Ø, Spencer J, Walsh TR, Lorentzen MS, Leiros H-KS.** 2013. Crystal structures of *Pseudomonas aeruginosa* GIM-1: active-site plasticity in metallo-β-lactamases. Antimicrob. Agents Chemother. **57:**848–854. http://dx.doi.org/10.1128/AAC.02227-12.
28. **Oelschlaeger P, Mayo SL.** 2005. Hydroxyl groups in the ββ sandwich of metallo-β-lactamases favor enzyme activity: a computational protein design study. J. Mol. Biol. **350:**395–401. http://dx.doi.org/10.1016/j.jmb.2005.04.044.
29. **Oelschlaeger P, Pleiss J.** 2007. Hydroxyl groups in the ββ sandwich of metallo-β-lactamases favor enzyme activity: Tyr218 and Ser262 pull down the lid. J. Mol. Biol. **366:**316–329. http://dx.doi.org/10.1016/j.jmb.2006.11.027.
30. **Oelschlaeger P, Mayo SL, Pleiss J.** 2005. Impact of remote mutations on metallo-β-lactamase substrate specificity: implications for the evolution of antibiotic resistance. Protein Sci. **14:**765–774. http://dx.doi.org/10.1110/ps.041093405.
31. **Merino M, Perez-Llarena FJ, Kerff F, Poza M, Mallo S, Rumbo-Feal S, Beceiro A, Juan C, Oliver A, Bou G.** 2010. Role of changes in the L3 loop of the active site in the evolution of enzymatic activity of VIM-type metallo-β-lactamases. J. Antimicrob. Chemother. **65:**1950–1954. http://dx.doi.org/10.1093/jac/dkq259.
32. **Zhang H, Hao Q.** 2011. Crystal structure of NDM-1 reveals a common β-lactam hydrolysis mechanism. FASEB J. **25:**2574–2582. http://dx.doi.org/10.1096/fj.11-184036.
33. **Materon IC, Palzkill T.** 2001. Identification of residues critical for metallo-β-lactamase function by codon randomization and selection. Protein Sci. **10:**2556–2565. http://dx.doi.org/10.1110/ps.ps.40884.
34. **Garau G, Garcia-Saez I, Bebrone C, Anne C, Mercuri P, Galleni M, Frere JM, Dideberg O.** 2004. Update of the standard numbering scheme for class B β-lactamases. Antimicrob. Agents Chemother. **48:**2347–2349. http://dx.doi.org/10.1128/AAC.48.7.2347-2349.2004.
35. **Wei LL, Cai XY, Qi ZG, Rong L, Cheng BJ, Fan J.** 2012. *In vivo* and *in vitro* characterization of TEV protease mutants. Protein Expr. Purif. **83:**157–163. http://dx.doi.org/10.1016/j.pep.2012.03.011.
36. **Cabrita LD, Gilis D, Robertson AL, Dehouck Y, Rooman M, Bottomley SP.** 2007. Enhancing the stability and solubility of TEV protease using *in silico* design. Protein Sci. **16:**2360–2367. http://dx.doi.org/10.1110/ps.072822507.
37. **van den Berg S, Lofdahl PA, Hard T, Berglund H.** 2006. Improved solubility of TEV protease by directed evolution. J. Biotechnol. **121:**291–298. http://dx.doi.org/10.1016/j.jbiotec.2005.08.006.
38. **Adams PD, Afonine PV, Bunkoczi G, Chen VB, Davis IW, Echols N, Headd JJ, Hung LW, Kapral GJ, Grosse-Kunstleve RW, McCoy AJ, Moriarty NW, Oeffner R, Read RJ, Richardson DC, Richardson JS, Terwilliger TC, Zwart PH.** 2010. PHENIX: a comprehensive Python-based system for

macromolecular structure solution. Acta Crystallogr. D Biol. Crystallogr. **66:** 213–221. http://dx.doi.org/10.1107/S0907444909052925.
39. **Collaborative Computational Project-4.** 1994. The CCP4 suite: programs for protein crystallography. Acta Crystallogr. D Biol. Crystallogr. **50:**760–763.
40. **Emsley P, Cowtan K.** 2004. Coot: model-building tools for molecular graphics. Acta Crystallogr. D Biol. Crystallogr. **60:**2126–2132. http://dx.doi.org/10.1107/S0907444904019158.
41. **Layton CJ, Hellinga HW.** 2010. Thermodynamic analysis of ligand-induced changes in protein thermal unfolding applied to high-throughput determination of ligand affinities with extrinsic fluorescent dyes. Biochemistry **49:**10831–10841. http://dx.doi.org/10.1021/bi101414z.
42. **Rasia RM, Vila AJ.** 2004. Structural determinants of substrate binding to *Bacillus cereus* metallo-β-lactamase. J. Biol. Chem. **279:**26046–26051. http://dx.doi.org/10.1074/jbc.M311373200.
43. **Spencer J, Read J, Sessions RB, Howell S, Blackburn GM, Gamblin SJ.** 2005. Antibiotic recognition by binuclear metallo-β-lactamases revealed by X-ray crystallography. J. Am. Chem. Soc. **127:**14439–14444. http://dx.doi.org/10.1021/ja0536062.
44. **Castanheira M, Deshpande LM, Mendes RE, Rodriguez-Noriega E, Jones RN, Morfin-Otero R.** 2011. Comment on: role of changes in the L3 loop of the active site in the evolution of enzymatic activity of VIM-type metallo-β-lactamases. J. Antimicrob. Chemother. **66:**684–686. (Letter.) http://dx.doi.org/10.1093/jac/dkq393.
45. **Concha NO, Janson CA, Rowling P, Pearson S, Cheever CA, Clarke BP, Lewis C, Galleni M, Frere JM, Payne DJ, Bateson JH, Abdel-Meguid SS.** 2000. Crystal structure of the IMP-1 metallo β-lactamase from *Pseudomonas aeruginosa* and its complex with a mercaptocarboxylate inhibitor: binding determinants of a potent, broad-spectrum inhibitor. Biochemistry **39:**4288–4298. http://dx.doi.org/10.1021/bi992569m.
46. **Yanchak MP, Taylor RA, Crowder MW.** 2000. Mutational analysis of metallo-β-lactamase CcrA from *Bacteroides fragilis*. Biochemistry **39:** 11330–11339. http://dx.doi.org/10.1021/bi0010524.
47. **Haruta S, Yamamoto ET, Eriguchi Y, Sawai T.** 2001. Characterization of the active-site residues asparagine 167 and lysine 161 of the IMP-1 metallo β-lactamase. FEMS Microbiol. Lett. **197:**85–89. http://dx.doi.org/10.1111/j.1574-6968.2001.tb10587.x.

Supplementary material to:

His224 alters the R2 drug binding site and Phe218 influences the catalytic efficiency in the metallo-β-lactamase VIM-7

Hanna-Kirsti S. Leiros, Susann Skagseth, Kine Susann Waade Edvardsen, Marit Sjo Lorentzen

Gro Elin Kjæreng Bjerga, Ingar Leiros and Ørjan Samuelsen

Table S1 *Steady state kinetic results for tVIM-7 (His-Tev-VIM-7 construct) and VIM-7 (native construct with the leader sequence).*

	tVIM-7			VIM-7			Ratio k_{cat}/K_m
	K_m	k_{cat}	k_{cat}/K_m	K_m	k_{cat}	k_{cat}/K_m	
Compound	**(μM)**	**(s^{-1})**	**($s^{-1} * \mu M^{-1}$)**	**(μM)**	**(s^{-1})**	**($s^{-1} * \mu M^{-1}$)**	**VIM-7/ tVIM-7**
Penicillins							
Benzylpenicillin [a]	23.1±3.2	59 ±7	2.5	13.8 ± 2.4	350 ± 17	25.4	10.2
Ampicillin [a]	23.3±1.7	17.6±1.1	0.76	0.56 ± 0.07	38 ± 9	67.9	89.3
Cephalosporins							
Cefepime	179±14	0.450±0.023	0.0025	14 ± 2	0.255± .008	0.018	7.2
Ceftazidime	61±19	0.120±0.007	0.0020	41.8 ± 2.6	0.186±0.005	0.0044	2.2
Cefoxitin	20±4	0.64±0.03	0.032	34 ± 3	37.51± 0.07	1.10	34.4
Cefuroxime	12.9±2.5	4.57±0.05	0.35	9.4 ± 0.8	9.9 ± 0.2	1.05	3.1
Carbapenems							
Ertapenem	18.9±2.2	12.810±0.013	0.68	10.6 ± 0.8	3.05 ± 0.05	0.280	0.4
Imipenem	29 ±10	7.71±0.17	0.27	12.4 ± 0.8	47.6 ± 0.5	3.84	14.2
Meropenem	20.0±1.6	25.580±0.026	1.28	22.4 ± 2.7	24.5 ± 0.5	1.09	0.85

[a] The K_m values were measured as inhibition constants (K_i) in a competitive model using nitrocefin as the reporter substrate.